Chinese Journal of
POLYMER SCIENCE

RESEARCH ARTICLE

https://doi.org/10.1007/s10118-024-3063-2
Chinese J. Polym. Sci. **2024**, *42*, 373–387

Molecular Dynamics Simulation Studies on the Micromorphology and Proton Transport of Nafion/$Ti_3C_2T_x$ Composite Membrane

Zhi-Yue Han[a], Su-Peng Pei[a*], Chun-Yang Yu[b,c*], and Yong-Feng Zhou[b,c]

[a] *School of Chemical and Environmental Engineering, Shanghai Institute of Technology, Shanghai 201418, China*
[b] *School of Chemistry & Chemical Engineering, Frontiers Science Center for Transformative Molecules, Shanghai Key Laboratory of Electrical Insulation and Thermal Aging, Shanghai Jiao Tong University, Shanghai 200240, China*
[c] *Key Laboratory of Green and High-end Utilization of Salt Lake Resources, Chinese Academy of Sciences, Xining 810008, China*

Electronic Supplementary Information

Abstract The perfluorosulfonic acid (PFSA) membrane doped with two-dimensional conductive filler $Ti_3C_2T_x$ is a fuel cell proton exchange membrane with high application potential. Experimental studies showed that the proton conductivity of Nafion/$Ti_3C_2T_x$ composite membrane is improved significantly compared with that in pure Nafion. However, the microscopic mechanism of doping on the enhancement of membrane performance is remain unclear now. In this work, molecular dynamics simulation was used to investigate the microscopic morphology and proton transport behaviors of Nafion/$Ti_3C_2T_x$ composite membrane at the molecular level. The results shown that there were significant differences about the diffusion kinetics of water molecules and hydroxium ions in Nafion/$Ti_3C_2T_x$ at low and high hydration levels in the nanoscale region. With the increase of water content, $Ti_3C_2T_x$ in membrane was gradually surrounded by ambient water molecules to form a hydration layer, and forming a relatively continuous proton transport channel between Nafion polymer and $Ti_3C_2T_x$ monomer. The continuous proton transport channel could increase the number of binding sites of proton and thus achieving high proton conductivity and high mobility of water molecules at higher hydration level. The current work can provide a theoretical guidance for designing new type of Nafion composite membranes.

Keywords Nafion/$Ti_3C_2T_x$ composite membrane; Proton transport; Molecular dynamics simulation

Citation: Han, Z. Y.; Pei, S. P.; Yu, C. Y.; Zhou, Y. F. Molecular dynamics simulation studies on the micromorphology and proton transport of Nafion/$Ti_3C_2T_x$ composite membrane. *Chinese J. Polym. Sci.* **2024**, *42*, 373–387.

INTRODUCTION

Proton exchange membrane fuel cell (PEMFC) has the advantages of small size, light weight, low exhaust emission and high energy conversion efficiency. It has been widely used in transportation applications, stationary applications and portable electronic devices.[1] Therefore, it has attracted the extensive attention from a great deal of researchers.[2–4] The proton exchange membrane (PEM) is the core device of PEMFC, which mainly plays the role of transferring protons, blocking electrons and isolating fuel, and is an important component of electrochemical reaction in membrane electrode assembly (MEA).[5] Among the various types of PEMs, the Nafion series of perfluorosulfonic acid (PFSA) membranes have been widely studied and applied due to high proton conductivity, good chemical and thermal stability.[6–8] It should be noted that the water and gas transmission processes involved in PEMs determine the overall performance of PEMFC. Therefore, the study of the transport process in hydrated Nafion membranes is of great significance to the operation of PEMFC.

With the increasing of application requirements, the performance specifications of PEMFC become getting higher. As with most polymer membranes, it is hard to improve the proton conductivity and mechanical stability of Nafion simultaneously, which limits its wide application.[9–11] In order to solve this problem, various methods such as doping and grafting strategies were tried to modify Nafion based membranes.[12–14] Compared with other methods, the doping method for Nafion is considered as an effective and practical strategy.[15,16] In recent years, Nafion based composite membranes formed by introducing ionic liquid, inorganic and organic dopants into Nafion matrix have been explored extensively. And studies have shown that the above doping methods could improve the comprehensive performance of Nafion membranes such as proton conductivity and mechanical property.[17–27]

Among the many doping materials, a promising method is to incorporate inorganic hydrophilic material MXene into the polymer matrix.[28] MXenes is a two-dimensional layered transition metal carbide, nitride and carbonitride material. Its gen-

* Corresponding authors, E-mail: peisupeng@126.com (S.P.P.)
E-mail: chunyangyu@sjtu.edu.cn (C.Y.Y.)

Received September 18, 2023; Accepted October 22, 2023; Published online November 21, 2023

eral molecular formula is: $M_{n+1}X_nT_x$ (n=1–4), where M is the transition metal, X is carbon (C) or nitrogen (N), T and x respectively represent its surface termination group and its number.[29] To date, $Ti_3C_2T_x$ is one of the typical materials of MXene, and the stripped $Ti_3C_2T_x$ layer is usually terminated by the —OH, —O— and/or —F groups. Due to its hydrophilic surface, large specific surface area, atomic scale thickness, high aspect ratio and other characteristics, $Ti_3C_2T_x$ has been explored for various water treatment, environmental and biomedical applications.[30–33] Meanwhile, the combination of MXene and PFSA shows excellent properties and has been explored for applications in PEMFC, optoelectronic applications and other fields. For example, Zhou *et al*.[34] combined a $Ti_3C_2T_x$ MXene thin film with PFSA barrier layer, as a transparent conductive electrodes (TCEs) material with excellent environmental stability. Wang *et al*.[35] demonstrated that the physical resistance of $Ti_3C_2T_x$ MXene and electrostatic repulsion of Nafion can synergistically inhibit the shuttle effect. Jang *et al*.[36] reported that Nafion@MXene/cellulose acetate (CA) composite cation exchange membrane (CEM) exhibits a higher power density than casted Nafion membrane. Tang *et al*.[37] reported that the blocking force of the MXene-Nafion composite actuator with a doping level of 0.5 wt% was about 6 times than that of the pure Nafion. Lee *et al*.[38] reported that the synergistic effect between $Ti_3C_2T_x$ MXene and mesoporous titania-Nafion composite film, which significantly increased the oxidation current towards capsaicin. Furthermore, compared to other two-dimensional (2D) materials such as graphene, $Ti_3C_2T_x$ can construct a wide and long proton transport path in membrane and is often used as a filler to modify PEM. MXene/PFSA composites as an enhanced PEM has also been explored for application in PEMFC. For instance, Zhang *et al*.[39] prepared PFSA/$Ti_3C_2T_x$ composite membrane and applied it to PEMFC to improve proton conductivity and thermo-mechanical stability. Liu *et al*.[40] incorporated $Ti_3C_2T_x$ into acidic Nafion phase separation, and found that the presence of inorganic filler $Ti_3C_2T_x$ enhanced proton conductivity and the overall properties of Nafion/$Ti_3C_2T_x$. This is expected to open up new prospects for Nafion membrane modifiers and proton conductors, and this research finding has also attracted our focus. In addition, many experimental techniques such as scanning electron microscopy (SEM), atomic force microscopy (AFM) and X-ray photoelectron spectroscopy (XPS) have been used to study Nafion/$Ti_3C_2T_x$. Nonetheless, the microscopic doping mechanism by which the presence of $Ti_3C_2T_x$ promotes proton transport remains unclear due to the limitation of the experimental measures.

As a supplement to the experiment, it is necessary to reveal the static and dynamic behavior of water and hydronium ions in polymer membranes through computer simulation.[41] Among various computer simulation techniques, molecular dynamics (MD) simulation is a suitable technique to determine the interactions between particles in a system, as well as the structure, interface, dynamics and mechanical properties of the system.[42,43] In addition, MD simulation has been widely used to study various properties of hydrated Nafion membranes, including structure and transport characteristics,[44–47] membrane morphology,[48–51] gas adsorption and permeation,[52–56] water adsorption and permeation,[57–61] and mechanical properties.[62–65] For example, Maiti *et al*.[66] studied the mechanical properties of SGO/PFSA composite membrane by MD simulation. Haghighi Asl *et al*.[67] investigated the organic-inorganic structure of UiO-66 MOF/Nafion, and its effects on the morphology of clusters and proton conductivity in the membrane by MD simulation. Liu *et al*.[68,69] studied the transport characteristics of water in 3M 825EW PFSA doped with HPAs and HPW by MD simulation. They found that the proton conductivity of the membrane increased at high relative humidity (RH), while the diffusion coefficient of water decreased. Akbari *et al*.[70,71] studied the proton transport characteristics of HPS, IPA and HPA-doped Nafion 117 membranes through MD simulation, and found that the proton mobility of the doped membranes increased at medium water content, while the mobility of water decreased. Moreover, they propose that the high proton conductivity and low water mobility of PFSA membranes doped with hydrophilic particles are two difficult objectives to reconcile. Although the above progress has been made on Nafion composite membranes, the theoretical study on MXene doping Nafion has not been reported.

Hence, in order to solve the above problems and further explore the microscopic doping mechanism of Nafion/$Ti_3C_2T_x$, we constructed $Ti_3C_2T_x$ containing adsorption groups and added it to the Nafion matrix. Then, the microscopic morphology and proton transport characteristics of Nafion/$Ti_3C_2T_x$ with different water contents were investigated by MD simulation. The existence of hydrophilic functional groups of $Ti_3C_2T_x$ packing was revealed at the molecular level, which formed a relatively continuous hydrogen bond network within membrane. And it is found that the proton transport environment in Nafion/$Ti_3C_2T_x$ was improved, while high proton conductivity and high mobility of water molecules were simultaneously achieved at higher hydration levels. The current work can provide a theoretical guidance for designing new type of Nafion composite membranes experimentally.

SIMULATION METHODS

Simulation Details

Model construction of Nafion, $Ti_3C_2T_x$ and Nafion/$Ti_3C_2T_x$

In this study, the EW=944 g/mol Nafion and the Nafion/$Ti_3C_2T_x$ composite membrane were constructed. Herein, PFSA membrane with EW=944 g/mol represents Nafion (5 wt% DE520) with EW=892–970 g/mol experimentally. The chemical structure of the Nafion polymer is shown in Fig. 1, with each Nafion chain containing 10 repeated monomers. And each repeated unit consists of 12 (x=5, y=1) —CF_2— groups in the main chain, 1 repeated unit (z=1) in the side chain. In addition, a single-layer $Ti_3C_2T_x$ nanosheet with a size of 2.1 nm × 2.4 nm was constructed, and its model and size setting was referred from the work of Lee *et al*.[72] (see Fig. 1). Moreover, the setting of the surface adsorption group of Ti_3C_2 was based on the experimental study of Liu *et al*.[40] and combined with the NMR analysis of Hope *et al*.,[73] where the ratio of O:F:OH was approximately 5:8:1.

For the composite model, a single-layer $Ti_3C_2T_x$ sheet was placed in the middle of a cubic box with a side length of 20 nm using Packmol software package.[74] And then 25 Nafion polymers were filled into the box containing $Ti_3C_2T_x$,

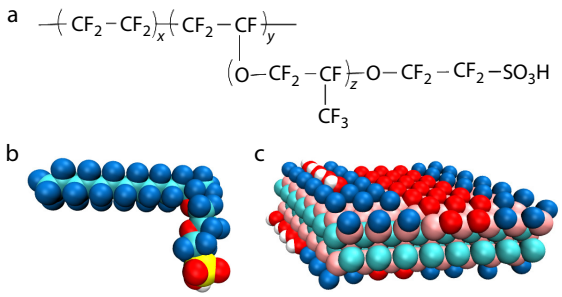

Fig. 1 Chemical formula (a), schematic structure (b) of Nafion chain, and the schematic structure of $Ti_3C_2T_x$ MXene that are used for the current simulation (c). The Ti, C, F, O, H and S atoms are represented by pink, cyan, blue, red, white and yellow, respectively.

where the mass percentage of $Ti_3C_2T_x$ was set to approximately 2.5 wt%. At the same time, different amounts of water molecules were put into the box to obtain PFSA membranes with different levels of hydration (λ=3, 6, 9, 12 and 20). Herein, λ is the water content of the membrane, expressed as the ratio of the number of water molecules to the number of SO_3^-. Finally, 250 hydrated protons were added to keep the system electrically neutral. It should be noted that it is assumed the sulfonic acid group in the side chain will be completely ionized to H^+ and SO_3^- when $\lambda \geq 3$ according to the study of Wang *et al.*[75] And the resulting protons combine with water and exist as hydronium ions (H_3O^+).

Force field parameter

The modified DREIDING force field of Mabuchi and Tokumasu[76] was employed for PFSA ionomer. F_3C water model[77] and classical hydronium model[78] were used for water and hydrated proton, respectively. Since there is no suitable force field that could describe the interaction between the various atoms in $Ti_3C_2T_x$ MXene, the universal force field[79] was used for $Ti_3C_2T_x$. In addition, the parameter setting of bond length and bond angle between surface Ti atom and adsorption group in $Ti_3C_2T_x$ was based on the work of Hu *et al.*[80] and the partial atomic charge were adapted from previous literatures.[81]

Simulation condition and procedure

All MD simulations were performed using GROMACS software[82] under three-dimensional periodic boundary conditions with a time step of 1 fs. Nose-Hoover thermostat[83] and Parrinello-Rahman[84] barostat were used to control the temperature and pressure of the simulation systems, respectively. In addition, the particle mesh Ewald (PME) method[85] was used to deal with the long-range electrostatic interaction, and the truncation distance of the van der Waals interaction and electrostatic interaction was 1.5 nm.

At the beginning of each simulation, 5000 steps of conjugate gradients were performed on the constructed structure to minimize potential energy. Subsequently, the systems were treated with the annealing method developed by Mabuchi and Tokumasu[76] to prevent the system from being in metastable state in order to obtain the initial configuration of MD simulation. And then the system was compressed to the experimental density by adjusting the LJ parameters under the NPT ensemble (Table S1 in the electronic supplementary information, ESI).

Quantum chemistry calculation

To quantitative investigate the interaction of sulfonic acid functional group-water and $Ti_3C_2T_x$-water, two interaction models were constructed. Then the geometries of all molecules were calculated through density functional theory (DFT). All the DFT computations were performed by the GB3LYP-D3 density functional method. The Def2-SVPD basis set was used for the energy calculation of all the model molecules in gas phase. All calculations are performed using BDF software on the Device Studio platform.[86–91]

RESULTS AND DISCUSSION

Equilibrium of Hydrated Nafion Membrane Systems

Equilibrium state of hydrated Nafion membranes

The equilibrium of the system is the precondition of data analysis in molecular dynamics simulation. Therefore, we firstly examine whether the equilibrium state is reached for each simulation system. Thus, the evolution of potential energy of hydrated Nafion membranes with simulation time was plotted. As shown in Fig. 2, the potential energy of the hydrated Nafion and Nafion/$Ti_3C_2T_x$ both fluctuate first and then tend to be stable under 50 ns, which indicate that the systems reached equilibrium.

Density of hydrated Nafion membranes

In order to further validate the reliability of the simulation sys-

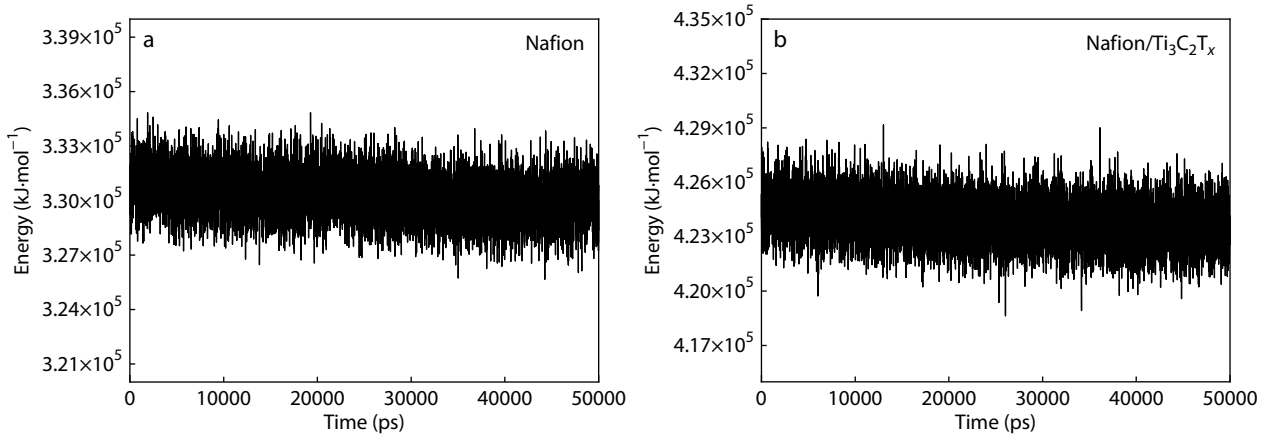

Fig. 2 Potential energy evolution diagram of (a) Nafion and (b) Nafion/$Ti_3C_2T_x$ simulation systems under 50 ns.

tems, the density of various hydrated Nafion and Nafion/$Ti_3C_2T_x$ membranes have been calculated on a basis of the equilibrium simulation data, and then compared them with the experimental data (Fig. 3). The experimental density of various membranes is obtained by the following fitting formula based on previous relevant studies:[92,93]

$$\rho = \frac{EW + M_{H_2O}\lambda}{V_m + \lambda V_{H_2O}} \quad (1)$$

where EW is the equivalent weight of Nafion ionomer, M_{H_2O} is the molecular weight of the water, λ is the water content, V_m is the partial molar volume of the dry Nafion membrane, which is calculated as $V_m = EW/\rho_m$, and ρ_m represents the density of the dry membrane (2.05 g/cm^3) in experiment, V_{H_2O} is the partial molar volumes of water, which is calculated as $V_{H_2O} = M_{H_2O}/\rho_{H_2O}$, and ρ_{H_2O} is the density of water.

As shown in Fig. 3, all the simulated density are generally in good agreement with the experimental value except for a slight deviation when the water content is 3, but the deviation is less than 5%. Meanwhile, the density of both Nafion and Nafion/$Ti_3C_2T_x$ membranes decreased with the increase of water content. And the density of Nafion/$Ti_3C_2T_x$ is higher than that of Nafion with different water contents.

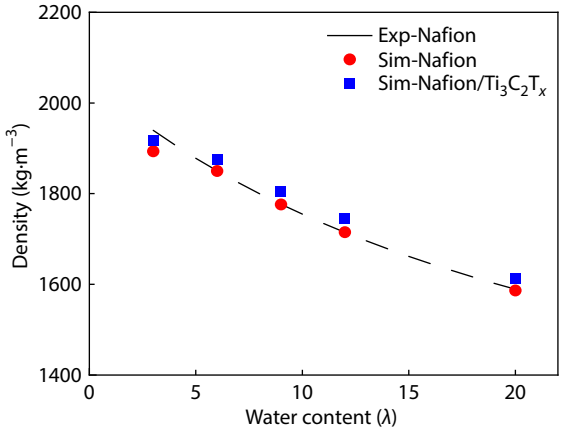

Fig. 3 Density of hydrated Nafion and Nafion/$Ti_3C_2T_x$ membranes at different water content.

Structure Analysis of Water Channels in Hydrated Nafion Membranes

The water channel structure in hydrated Nafion membrane plays a crucial role in the proton transport process. However, the structure of the water channels in membrane with different water contents is not exactly the same. Therefore, the radial distribution function (RDF) combined with coordination number (CN) were used to analyse the morphology of Nafion and Nafion/$Ti_3C_2T_x$ membranes with different water contents. Furthermore, the effect of adding $Ti_3C_2T_x$ to Nafion matrix on water distribution was investigated.

Local microstructure around sulfonic acid groups in hydrated Nafion membranes

The negative charged sulfonic acid groups in the side chain of Nafion polymers have adsorption effect on water, which affects the distribution of water molecules and hydrated protons in membranes. Therefore, the RDFs between sulfonic acid groups and sulfonic acid groups, water molecules, hydronium are employed to characterize the distribution around sulfonic acid groups in Nafion and Nafion/$Ti_3C_2T_x$ (Fig. 4).

As shown in Figs. 4(a) and 4(b), the characteristic distance between sulfur atoms in Nafion and Nafion/$Ti_3C_2T_x$ is 4.52 Å. This indicates that ionic clusters can be formed despite electrostatic repulsion between sulfonic acid groups in Nafion and Nafion/$Ti_3C_2T_x$. Figs. 4(c)–4(f) show that the characteristic distance between sulfur atoms and oxygen atoms on water molecules/hydronium in Nafion is 4.02 Å. And the first peak in Nafion/$Ti_3C_2T_x$ shifts slightly to 4.04 Å (Figs. 4d and 4f). This indicates that the addition of $Ti_3C_2T_x$ has little effect on the distribution of water molecules and hydronium around sulfonic acid groups. In addition, the positions of the second peak in Nafion and Nafion/$Ti_3C_2T_x$ are slightly shifted to the left while the water content is 3 (Figs. 4e and 4f). It is because hydrated protons are closely bound to the sulfonic groups when the water content is lower. Meanwhile, a decrease in peak height of RDFs for Nafion and Nafion/$Ti_3C_2T_x$ as the water content increases was observed (Figs. 4a–4f). In short, the distribution of RDFs between sulfonate groups and other atoms in pure Nafion is consistent with previous studies.[76,94,95] However, given the difference in number density of different systems,[96] the above studies cannot be used to reveal the influence of the water content. In order to further reveal the variation trend of the coordination environment of sulfonic acid groups in Nafion and Nafion/$Ti_3C_2T_x$, the CN for other atoms around sulfur atoms is summarized in Table 1.

The CN for the S-S pair is defined as the number of sulfur atoms within 6.50 Å around any given sulfur atoms. As shown in Table 1, the CN of the S-S pair in Nafion and Nafion/$Ti_3C_2T_x$ both decreases with the increasing water content. It is mainly due to the gradual dissolution of sulfonic acid groups in membranes as water content increases. In addition, the CN for the S-S pair of Nafion/$Ti_3C_2T_x$ is slightly lower than that of Nafion at low water content (λ=3, 6), indicating that the polymer chain in membrane is relatively compact. However, the opposite is true while the water content is higher (λ=9, 12 and 20), which indicates that the individual polymer chain is relatively stretched at this time. Moreover, the CN for the S-OW pair is defined as the number of oxygen atoms on water molecules within 4.70 Å around any given sulfur atoms. Thus, the distance 4.70 Å was chosen as the end of the first peak in RDF between sulfonic acid groups and water molecules.[95] As shown in Table 1, the CN for the S-OW pair in Nafion and Nafion/$Ti_3C_2T_x$ increases as the water content increases. Moreover, although the CN for the S-OW pair is not much different in Nafion and Nafion/$Ti_3C_2T_x$, it is slightly lower in Nafion/$Ti_3C_2T_x$ than that in Nafion. It is because the fluidity of water gradually increases as increased water content, resulting in the relative weakening of the binding strength of water molecules and sulfonic acid groups in Nafion/$Ti_3C_2T_x$. Meanwhile, the CN for the S-OH pair is defined as the number of oxygen atoms on hydronium within 4.70 Å around any given sulfur atoms. As shown in Table 1, the CN for the S-OH pair in Nafion and Nafion/$Ti_3C_2T_x$ are gradually reduced with increasing water content. It is because the protons dissolve in water and are gradually dispersed in membranes. And the CN of the S-OH pair is slightly higher in Nafion/$Ti_3C_2T_x$ than that in Nafion at higher water contents (λ=9, 12 and 20). It once

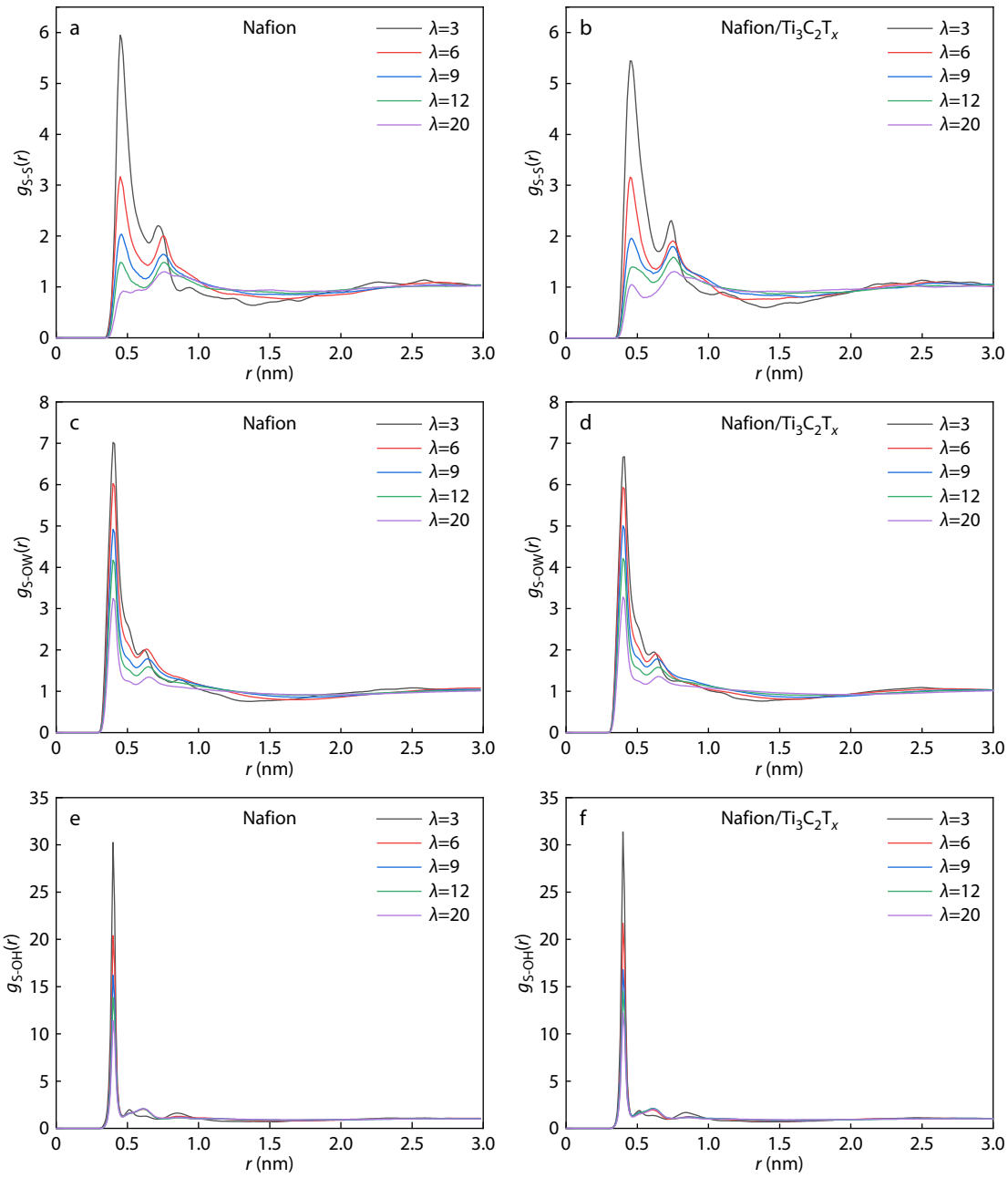

Fig. 4 RDF for (a, b) S-S (sulfur atoms on polymer), (c, d) S-OW (oxygen atoms on water molecules), (e, f) S-OH (oxygen atoms on hydronium) in Nafion and Nafion/$Ti_3C_2T_x$ with different water contents.

Table 1 Coordination number for sulfur atoms, oxygen atoms on water molecules, oxygen atoms on hydronium around sulfur atoms in Nafion and Nafion/$Ti_3C_2T_x$ with different water contents.

g (r)	System	λ=3	λ=6	λ=9	λ=12	λ=20
S-S	Nafion	3.12	1.60	1.05	0.71	0.20
	Nafion/$Ti_3C_2T_x$	3.07	1.58	1.06	0.74	0.25
S-OW	Nafion	2.95	5.64	6.66	7.13	7.85
	Nafion/$Ti_3C_2T_x$	2.72	5.39	6.62	7.03	7.79
S-OH	Nafion	2.63	1.78	1.33	1.07	0.75
	Nafion/$Ti_3C_2T_x$	2.63	1.77	1.34	1.08	0.78
OH-OW	Nafion	1.86	3.43	4.15	4.59	5.21
	Nafion/$Ti_3C_2T_x$	1.83	3.30	4.08	4.51	5.17

https://doi.org/10.1007/s10118-024-3063-2

again proves that the addition of $Ti_3C_2T_x$ has little effect on the distribution of hydronium around sulfonic acid groups.

In conclusion, the RDF analysis proved that sulfonic acid groups on the side chain of Nafion can adsorbed water molecules and hydrated protons to form a hydrophilic area in membranes. The addition of $T_3C_2T_x$ to Nafion has little effect on the distribution of water molecules and hydronium around sulfonic acid groups in membrane.

Local microstructure in water channels in hydrated Nafion membranes

In order to further explore the interaction and relative distribution of hydronium and water molecules in water channels in Nafion and Nafion/$Ti_3C_2T_x$, the RDFs between oxygen atoms on hydronium and oxygen atoms on water molecules are subsequently analyzed (Fig. 5). Meanwhile, in order to reveal the variation trend of the coordination environment of oxygen atoms on hydronium with different water contents, the CN for oxygen atoms on water molecules around oxygen atoms on hydronium is also listed in Table 1.

As shown in Figs. 5(a) and 5(b), the characteristic distance between oxygen atoms on hydronium and oxygen atoms on water molecules in Nafion is 2.73 Å, which is similar to the study by Ohkubo *et al*.[94] However, the position of the first peak in Nafion/$Ti_3C_2T_x$ shifts slightly to 2.71 Å in Nafion/$Ti_3C_2T_x$. It indicates that the addition of $Ti_3C_2T_x$ has little effect on the distribution of water molecules around hydronium. And it is observed that the peak height of both reduces as the water content increases. Furthermore, the CN for the OH-OW pair is defined as the number of oxygen atoms on water molecule within 3.70 Å around any given oxygen atoms on hydronium. As shown in Table 1, the CN for the OH-OW pair in Nafion and Nafion/$Ti_3C_2T_x$ gradually increases with increasing water content. It is because the protons dissolve in water and are gradually dispersed in membranes. And the CN of the OH-OW pair is slightly smaller in Nafion/$Ti_3C_2T_x$ than in Nafion as the water content increases. It shows that the fluidity for hydronium and water molecules is stronger in Nafion/$Ti_3C_2T_x$.

The static structure factor was further calculated as the Fourier transform of the radial distribution function to reveal the structure information at the large scales. As shown in Fig. S1 (in ESI), the ionomer peak position shifts to smaller values of q with increasing water content in Nafion and Nafion/$Ti_3C_2T_x$. In addition, the values of q for Nafion/$Ti_3C_2T_x$ are smaller than that of Nafion at high water contents. That is to say, the phase separation scale for Nafion/$Ti_3C_2T_x$ is larger than that of Nafion, which is more conducive to proton transport. It should be noted the smaller value of q corresponds to the larger phase separation at λ=20 was not obtained in Nafion and Nafion/$Ti_3C_2T_x$ due to the limitation of the simulation box size.

In summary, the addition of $Ti_3C_2T_x$ into the Nafion matrix has little effect on the distribution of water molecules and hydronium ions around sulfonic acid groups, as well as the mutual distribution between water molecules and hydronium ions. Moreover, the values of q are smaller and the phase separation size is larger for Nafion/$Ti_3C_2T_x$ than that of Nafion at high water content. Furthermore, the addition of $Ti_3C_2T_x$ promotes the flow of water molecules and hydronium in Nafion. The specific details will be further analyzed and discussed below.

Chain Length Analysis in Hydrated Nafion Membranes

The water distribution in hydrated Nafion membranes can affect the distribution of polymer chains in membranes under different water content. Thereby impact the proton transport process in membrane. Moreover, the radius of gyration (Rg) reflects the degree of curvation of the polymer and can represent the molecular size of the polymer as a whole. Therefore, the values of Rg for Nafion and Nafion/$Ti_3C_2T_x$ were calculated, and then the distribution of polymer chains in membranes is analysed.

The average values of Rg and the total values of Rg, corresponded to the Rg values of a single polymer chain and all polymer in Nafion and Nafion/$Ti_3C_2T_x$, are respectively calculated to describe the stretch of the polymer chain in the membrane (Fig. 6). As shown in Fig. 6(a), the average values of Rg for Nafion/$Ti_3C_2T_x$ are slightly lower than that of the Nafion at low water content (λ=3, 6). This maybe because the sulfonic acid groups bond relatively tighter at low water content, so the polymer chain shows a relatively compact state. However, the average values of Rg for Nafion/$Ti_3C_2T_x$ are larger than that of Nafion at higher water contents (λ=9, 12 and

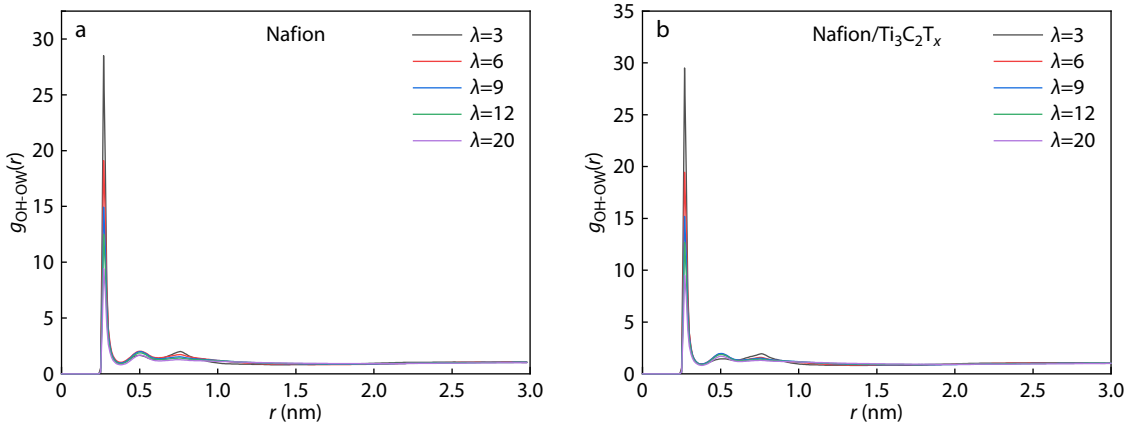

Fig. 5 RDF for OH-OW(oxygen atoms on hydronium-oxygen atoms on water molecules) in (a) Nafion and (b) Nafion/$Ti_3C_2T_x$ with different water contents.

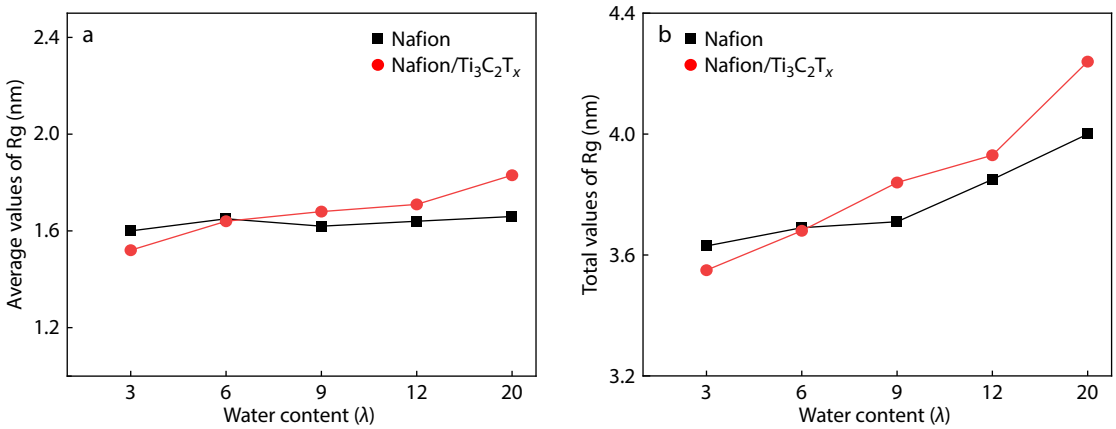

Fig. 6 Average values of Rg (a), total values of Rg (b) for Nafion and Nafion/$Ti_3C_2T_x$ with different water contents. The average values of Rg and the total values of Rg, corresponded to the Rg values of a single polymer chain and all polymer chains in Nafion and Nafion/$Ti_3C_2T_x$.

20), indicating that the polymer chain in Nafion/$Ti_3C_2T_x$ becomes more stretched in this time. The phenomenon may be due to the addition of $Ti_3C_2T_x$ to make the spatial distribution range of water larger in membrane.

Meanwhile, there is a certain interaction between sulfonic acid groups and water, which makes the polymer chain more stretched with increasing water content. To quantitative investigate the interaction of sulfonic acid functional group-water and $Ti_3C_2T_x$-water, the interaction energy between them was calculated. As shown in Fig. 7, both sulfonic acid groups and $Ti_3C_2T_x$ can form a stable adsorption structure. And the interaction energies of sulfonic acid functional group-water and $Ti_3C_2T_x$-water are −17.27 and −10.64 kcal/mol, respectively. This means that $Ti_3C_2T_x$ in Nafion/$Ti_3C_2T_x$ can adsorb water molecules. Specifically, there are adsorptions between fluorine atoms, oxygen atoms on the surface of $Ti_3C_2T_x$ and water molecules.

In addition, the total values of Rg in Nafion and Nafion/$Ti_3C_2T_x$ also conform to the above change rules. Compared with pure Nafion, the changes in total values of Rg for Nafion/$Ti_3C_2T_x$ is slightly obvious at higher water content. The results are consistent with the calculation result of the RDFs and CN between sulfonic acid groups in Fig. 4 and Table 1.

What's more, in order to more intuitively observe the microscopic morphological changes of polymer chains at different water contents, the distribution of water within 15 Å around the polymer chains in Nafion and Nafion/$Ti_3C_2T_x$ is shown in Fig. 8. We can see that the water distribution around the polymer chain in Nafion/$Ti_3C_2T_x$ at λ=3 is relatively concentrated, and the polymer chain is more compact compared with that in pure Nafion. However, the water molecules in Nafion/$Ti_3C_2T_x$ are more extensively distributed along the polymer chain, and then the polymer chain is more stretched while λ=9, 12 and 20.

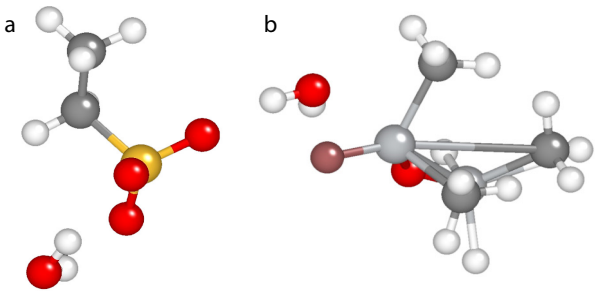

Fig. 7 The interaction models of sulfonic acid functional group-water (a), and $Ti_3C_2T_x$-water (b). The Ti, C, O, H, S and F atoms are represented by light grey, dark grey, red, white, yellow and brown, respectively.

Morphological Distribution of Water Clusters in Hydrated Nafion Membranes

The morphology of water clusters in hydrated Nafion membranes affects the connection and distribution of aqueous domain to a certain extent, and then affects the water channel structure in membranes. Therefore, the water volume (WV), the surface area (SA) of water and polymer boundary interface and the total volume (TV) of membranes were used to quantitatively characterize the geometry and distribution of aqueous domain in membranes. Among them, the ratio of SA to TV and SA to WV were used to describe the distribution and morphology of aqueous domain in hydrated Nafion membranes, respectively. On the one hand, the larger SA/TV ratio indicates that the spatial distribution of water in membrane is more widespread. On the other hand, a lower SA/WV manifests that the water clusters tend to have a larger size.

As shown in Fig. 9(a), the SA/WV ratio in Nafion and Nafion/$Ti_3C_2T_x$ gradually decreases with increasing water content, which shows that water molecules aggregate into clusters and tended to have a larger size at higher hydration levels. In addition, the SA/WV ratio of Nafion/$Ti_3C_2T_x$ is lower than that of Nafion, which is attributed that both $Ti_3C_2T_x$ and Nafion polymer chains have a certain adsorption effect on water in Nafion/$Ti_3C_2T_x$, and the water clusters have a tendency to form larger sizes.

Moreover, the SA/TV ratio of Nafion and Nafion/$Ti_3C_2T_x$ all gradually increases as water content increases, as shown in Fig. 9(b). It shows that the distribution range of water in membranes becomes more extensive as water content increases. The SA/TV ratio of Nafion/$Ti_3C_2T_x$ is lower than that of Nafion while the water content is low to 3 and 6. It may be because the number of water molecules is little at lower water content. Meanwhile, both Nafion polymer chains and $Ti_3C_2T_x$ adsorbed water molecules to a certain extent. This results in a

https://doi.org/10.1007/s10118-024-3063-2

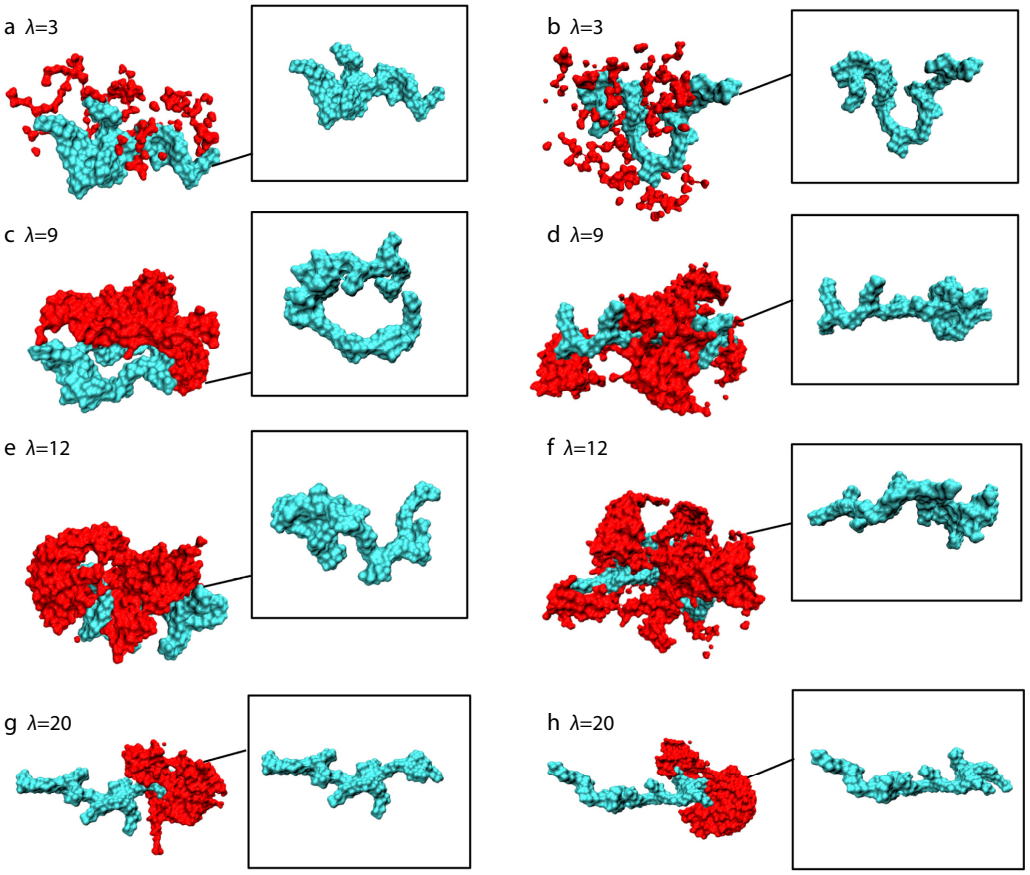

Fig. 8 Diagram of water distribution within 15 Å around polymer chains in (a, c, e, g) Nafion and (b, d, f, h) Nafion/$Ti_3C_2T_x$ at λ=3, 9, 12 and 20. Water clusters and polymer chains are represented by red and cyan, respectively.

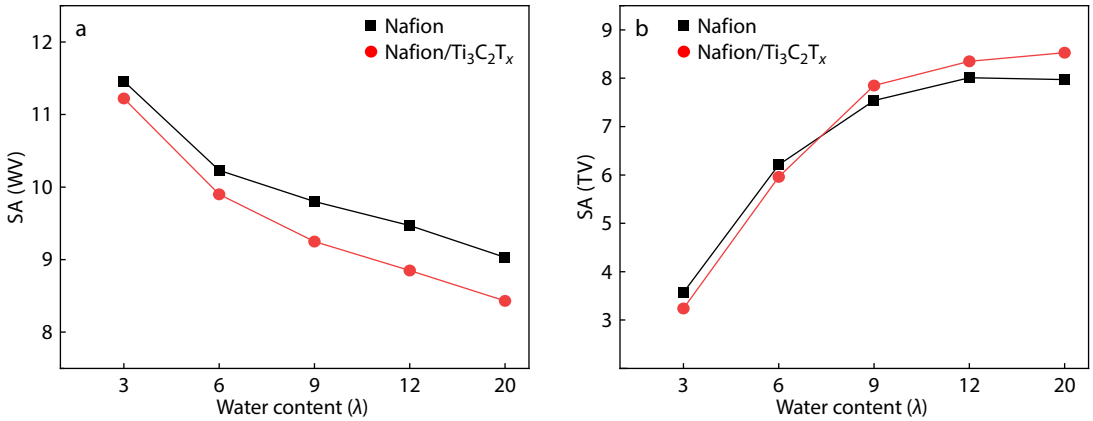

Fig. 9 The (a) SA/WV and (b) SA/TV for Nafion and Nafion/$Ti_3C_2T_x$ with different water contents.

relatively concentrated state of water in membranes as a whole. And the above results are consistent with the Rg values of a single polymer chain and the total polymers in Nafion and Nafion/$Ti_3C_2T_x$ calculated in Fig. 6. And the above analysis results are also corresponded to the diagram of water distribution within 15 Å around polymer chains in Nafion and Nafion/$Ti_3C_2T_x$ shown in Figs. 8(a) and 8(b). However, the SA/TV in Nafion/$Ti_3C_2T_x$ is higher and SA/WV is lower at higher water content compared with Nafion. The above results show that water molecules in Nafion/$Ti_3C_2T_x$ is not distributed discretely but have a wider continuous spatial distribution. And water molecules in Nafion/$Ti_3C_2T_x$ tend to form larger water clusters or even aggregate to form a hydration layer. This analysis results are also corresponded to the diagram of water distribution within 15 Å around polymer chains in Nafion and Nafion/$Ti_3C_2T_x$ shown in Figs. 8(c)–8(h).

Influence of $Ti_3C_2T_x$ on Local Microstructure in Water Channels in Nafion/$Ti_3C_2T_x$

Based on the above research on the structure analysis of water channels in hydrated Nafion membranes, it is found that the addition of $Ti_3C_2T_x$ into Nafion can promote the fluidity of water

https://doi.org/10.1007/s10118-024-3063-2

molecules and hydronium in Nafion/$Ti_3C_2T_x$. Therefore, in order to further explore the influence of the addition of $Ti_3C_2T_x$ on the internal microstructure of water channels, the water distribution around $Ti_3C_2T_x$ in Nafion/$Ti_3C_2T_x$ was investigated.

Water distribution analysis around $Ti_3C_2T_x$

In order to explore the water distribution around $Ti_3C_2T_x$ in Nafion/$Ti_3C_2T_x$, the RDFs between fluorine atoms (F), oxygen atoms (O) on the surface of $Ti_3C_2T_x$ and oxygen atoms on water/hydronium are analyzed (Fig. 10). As well, in order to reveal the variation trend of the coordination environment of fluorine atoms, oxygen atoms on $Ti_3C_2T_x$ with different water contents, the relevant CN is listed in Table 2.

As shown in Figs. 10(a) and 10(c), the characteristic distance between fluorine atoms, oxygen atoms on $Ti_3C_2T_x$ and oxygen atoms on water molecules in Nafion/$Ti_3C_2T_x$ is 2.90 Å and 3.10 Å, respectively. As shown in Table 2, the CN for the F-OW pair is defined as the number of oxygen atoms on water molecules within 4.00 Å around any given fluorine atoms on $Ti_3C_2T_x$. And the CN for the O-OW pair is defined as the number of oxygen atoms on water molecules within 4.30 Å around any given oxygen atoms on $Ti_3C_2T_x$. The results indicate that $Ti_3C_2T_x$ has a certain degree of adsorption on water, which have been revealed in Fig. 7. In addition, the characteristic distance between fluorine atoms on $Ti_3C_2T_x$ and oxygen atoms on water molecules is smaller than that between oxygen atoms on $Ti_3C_2T_x$ and oxygen atoms on water molecules. Moreover, the CN for the F-OW pair and the O-OW pair gradually increases with increasing water content. And the CN of the F-OW pair is always higher than that of the O-OW pair at different water content. The above results mean that the coordination between fluorine atoms on $Ti_3C_2T_x$ and oxygen atoms on water molecules is relatively stronger.

As shown in Figs. 10(b) and 10(d), the characteristic distance between fluorine atoms, oxygen atoms on $Ti_3C_2T_x$ and oxygen atoms on hydronium in Nafion/$Ti_3C_2T_x$ appear near 3.00 and 3.20 Å, respectively. As shown in Table 2, the CN for the F-OH pair and the O-OH pair is defined as the number of oxygen atoms on hydronium within 4.00 Å around any given fluorine and oxygen atoms on $Ti_3C_2T_x$, respectively. And the CN of the F-OH pair is slightly higher than that of the O-OH pair at different water content. It can be seen that the coordination between fluorine atoms on $Ti_3C_2T_x$ and oxygen atoms on hydronium is stronger. Furthermore, there are three obvious peaks between fluorine atoms, oxygen atoms on $Ti_3C_2T_x$ and oxygen atoms on water molecules, hydronium at low water content. However, the third coordination layer gradually disappeared with the continuous increasing water content. In addition, it can be seen that the CN for the F-OH pair and the O-OH pair is gradually reduced as the water content increases, the CN of both is close to 0 while λ=20 (Table 2). The above are because most protons are gradually dissolved in water and coordinate with water with increasing water content,

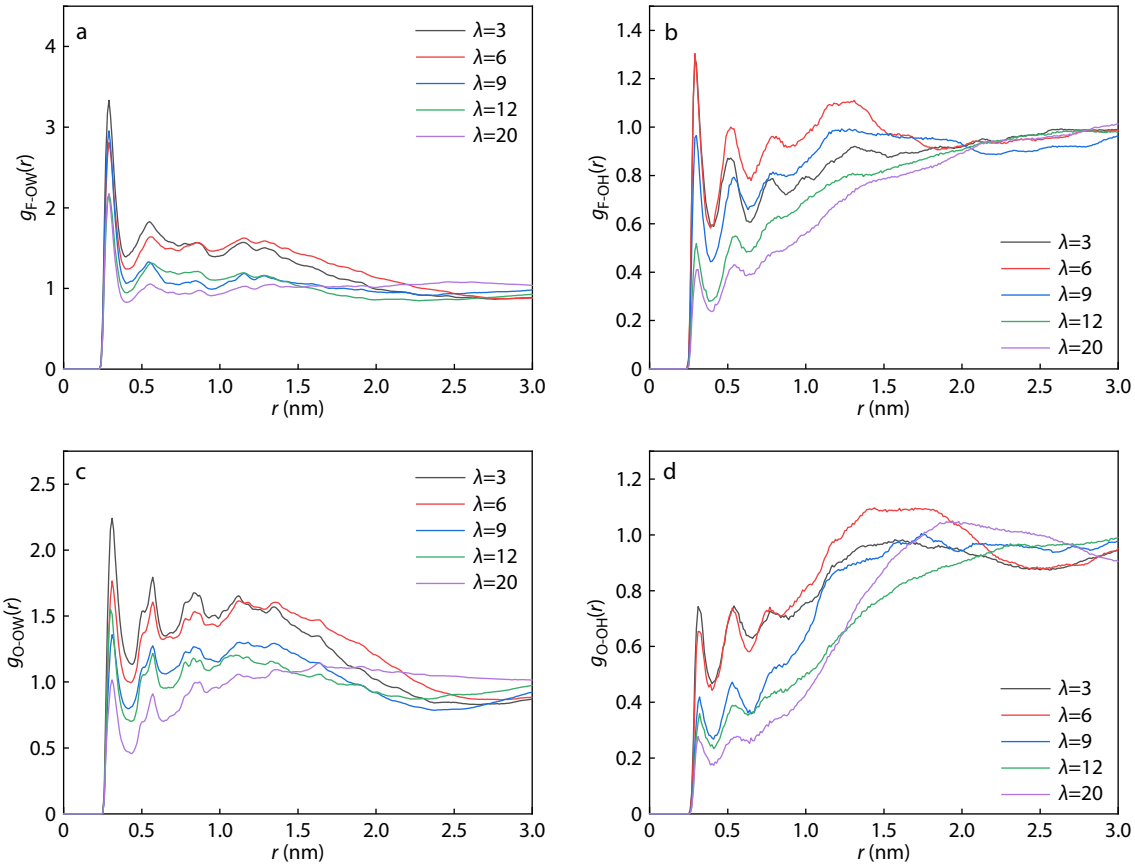

Fig. 10 RDF for (a) F-OW (fluorine atoms on $Ti_3C_2T_x$ and oxygen atoms on water molecules), (b) F-OH (fluorine atoms on $Ti_3C_2T_x$ and oxygen atoms on hydronium), (c) O-OW (oxygen atoms on $Ti_3C_2T_x$ and oxygen atoms on water molecules), (d) O-OH (oxygen atoms on $Ti_3C_2T_x$ and oxygen atoms on hydronium).

https://doi.org/10.1007/s10118-024-3063-2

Table 2 Coordination number for water/hydronium oxygen atoms around fluorine and oxygen atoms on $Ti_3C_2T_x$ with different water contents.

g(*r*)	λ=3	λ=6	λ=9	λ=12	λ=20
F-OW	0.95	2.14	2.67	2.72	3.02
F-OH	0.23	0.15	0.14	0.13	0.05
O-OW	0.78	1.82	1.99	2.31	2.75
O-OH	0.12	0.10	0.10	0.08	0.03

thus playing the role of bridging sulfonic acid groups to form clusters.

Interaction energy between $Ti_3C_2T_x$ and water molecules

In order to further explore the interaction strength between $Ti_3C_2T_x$ and water molecules in Nafion/$Ti_3C_2T_x$ with different water contents, the interaction energy between $Ti_3C_2T_x$ monomer and water molecules is calculated.

As shown in Fig. 11, the negative value indicates that there is an attraction between the $Ti_3C_2T_x$ and water molecules. And the interaction between $Ti_3C_2T_x$ and water molecules was gradually enhanced with increasing water content.

Furthermore, so as to more intuitively observe the water distribution around $Ti_3C_2T_x$ with different water contents, the diagram of water distribution within 15 Å around $Ti_3C_2T_x$ in Nafion/$Ti_3C_2T_x$ is shown in Fig. 12. It can be observed from Fig. 12 that $Ti_3C_2T_x$ in Nafion/$Ti_3C_2T_x$ is gradually surrounded by ambient water molecules to form a hydration layer as water content increases. And a relatively continuous proton transport channel between Nafion polymer and $Ti_3C_2T_x$ monomer are formed. This indicates that the adsorption effect of $Ti_3C_2T_x$ on water molecules becomes stronger with the increased water content, which is consistent with the calculation result of the interaction energy between $Ti_3C_2T_x$ and water shown in Fig. 11. And it is further proved that the $Ti_3C_2T_x$ added into the Nafion matrix has a certain hydrophilicity, which is correspond to the experimental results.[97]

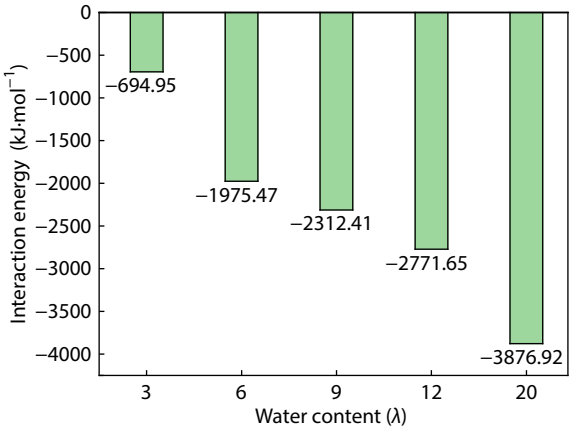

Fig. 11 Interaction energy between $Ti_3C_2T_x$ and water molecules in Nafion/$Ti_3C_2T_x$ with different water contents.

Hydrogen Bonds Kinetics of Hydrated Nafion Membranes

In the hydrated Nafion membranes, the hydrogen bonds network is an important carrier for the transport of water molecules and hydronium, and plays an important role in the proton transport process. Therefore, the number and lifetime of hydrogen bonds in Nafion and Nafion/$Ti_3C_2T_x$ were analyzed to explore the influence of hydrogen bond dynamics on the diffusion kinetics of water and hydronium.

As shown in Fig. 13, the total number of hydrogen bonds in Nafion and Nafion/$Ti_3C_2T_x$ increase gradually with increasing water content. Moreover, the total number of hydrogen bonds in Nafion/$Ti_3C_2T_x$ is lower than that in Nafion at lower water content (λ=3, 6). This is because the number of water molecules is relatively small when the water content is low, and the $Ti_3C_2T_x$ and Nafion have adsorption effects on water molecules. It results in the formation of a hydrogen bond network with poorer connectivity in Nafion/$Ti_3C_2T_x$ than that in Nafion. However, the total number of hydrogen bonds in Nafion/$Ti_3C_2T_x$ is higher than that in Nafion at higher water content (λ=9, 12 and 20). This is because a more continuous hydrogen bond network structure is formed in Nafion/$Ti_3C_2T_x$, which improves the proton transport environment within the membrane.

Hydrogen bonds lifetime analysis of hydrated Nafion membranes

As shown in Fig. 14, the hydrogen bonds lifetime of water-hydronium, water/hydronium-Nafion and water/hydronium-Nafion/$Ti_3C_2T_x$ all decrease gradually with increasing water content. This is due to the acceleration of the fluidity of water and hydrated protons as water content increases. In addition, the lifetime of all hydrogen bonds in Nafion/$Ti_3C_2T_x$ is higher than

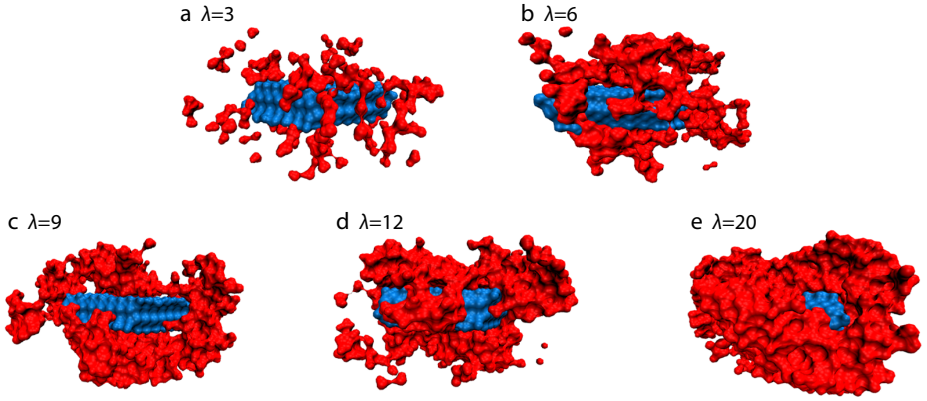

Fig. 12 Diagram of water distribution within 15 Å around $Ti_3C_2T_x$ in Nafion/$Ti_3C_2T_x$ with different water contents. Water clusters and $Ti_3C_2T_x$ are represented by red and blue, respectively.

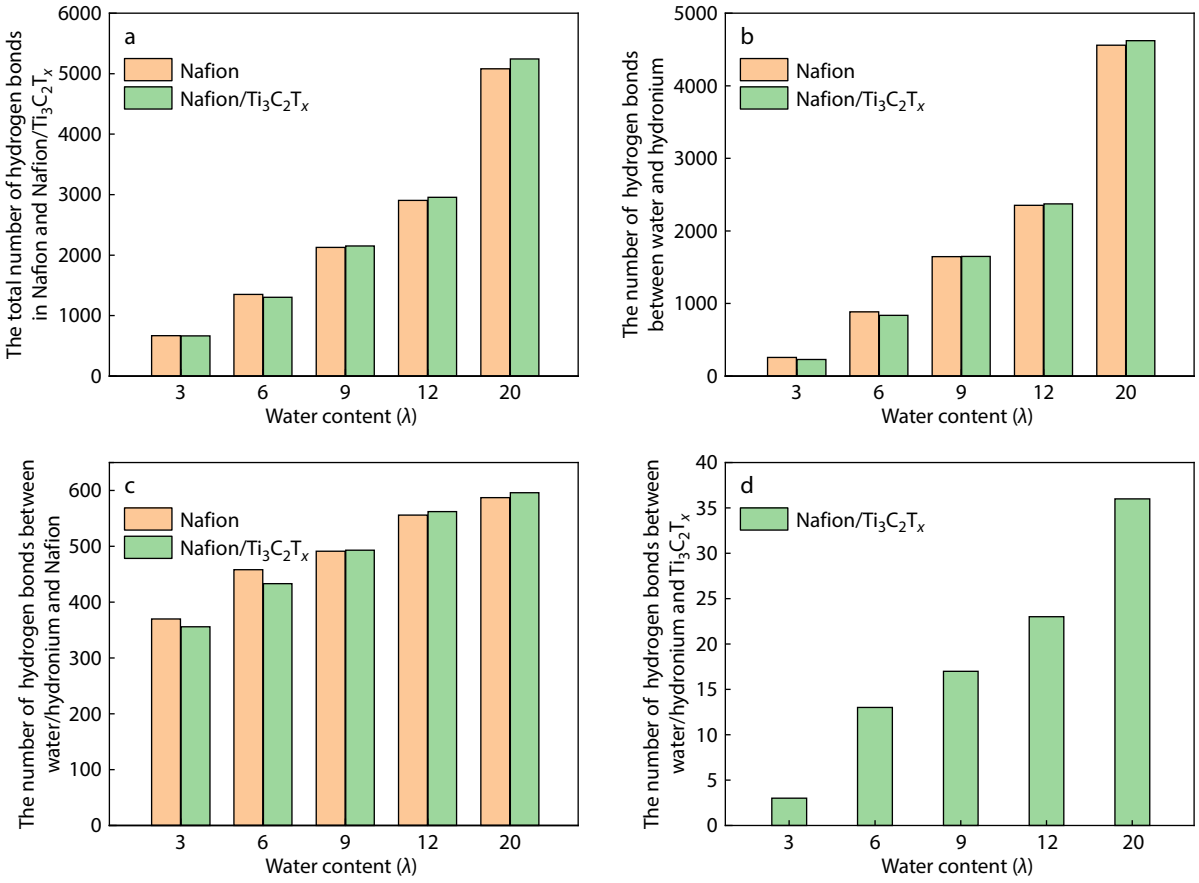

Fig. 13 The total number of hydrogen bonds (a), the number of hydrogen bonds between water and hydronium (b), water/hydronium and Nafion (c), water/hydronium and $Ti_3C_2T_x$ (d) in Nafion and Nafion/$Ti_3C_2T_x$ with different water contents.

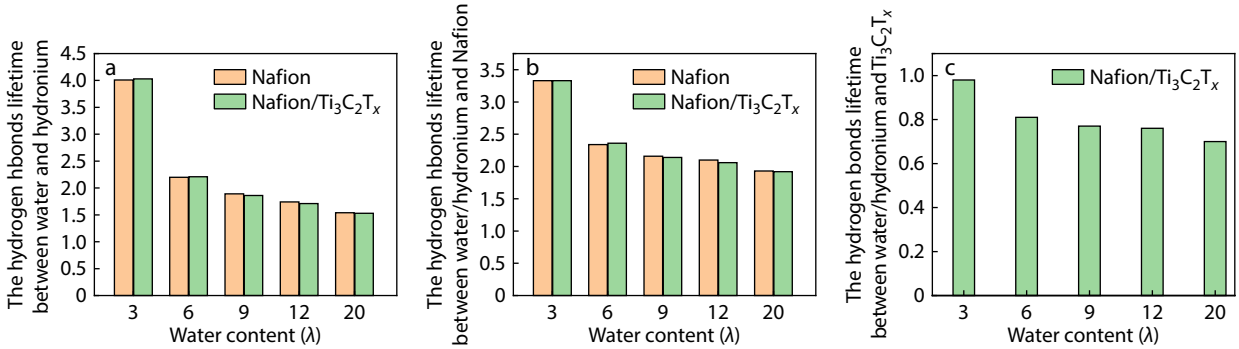

Fig. 14 The hydrogen bonds lifetime between water and hydronium (a), water/hydronium and Nafion (b), water/hydronium and $Ti_3C_2T_x$ (c) in Nafion and Nafion/$Ti_3C_2T_x$ with different water contents.

that of Nafion at lower water content (λ=3, 6). This is due to the poor connectivity of the hydrogen bonds network, and the slower mobility of water and hydrated protons in Nafion/$Ti_3C_2T_x$ than that in Nafion. However, the opposite is true at higher water content (λ=9, 12 and 20). A possible explanation was reported by Devanathan *et al.*[98] that a relatively continuous three-dimensional percolating water network is gradually formed as increasing water content. The relatively continuous water network can accelerate the water and hydrated protons transfer. This further indicates that the hydrophilic material $Ti_3C_2T_x$ improves the water and hydrated protons transport environment in membrane.

Furthermore, the average hydrogen bonds lifetime of water/hydronium-$Ti_3C_2T_x$ is decreased gradually with increasing water content (Fig. 14c). And it is lower than the average of hydrogen bonds lifetime of water-hydronium, water/hydronium-Nafion. It means that the water environment around $Ti_3C_2T_x$ is well distributed, and the continuity of the proton transport channel is better. To sum up, the investigation on hydrogen bonds kinetics of hydrated Nafion membranes further prove that the addition of $Ti_3C_2T_x$ can improve the distribution of water environment. And then the fluidity of water molecules and hydrated protons in membrane can be enhanced.

https://doi.org/10.1007/s10118-024-3063-2

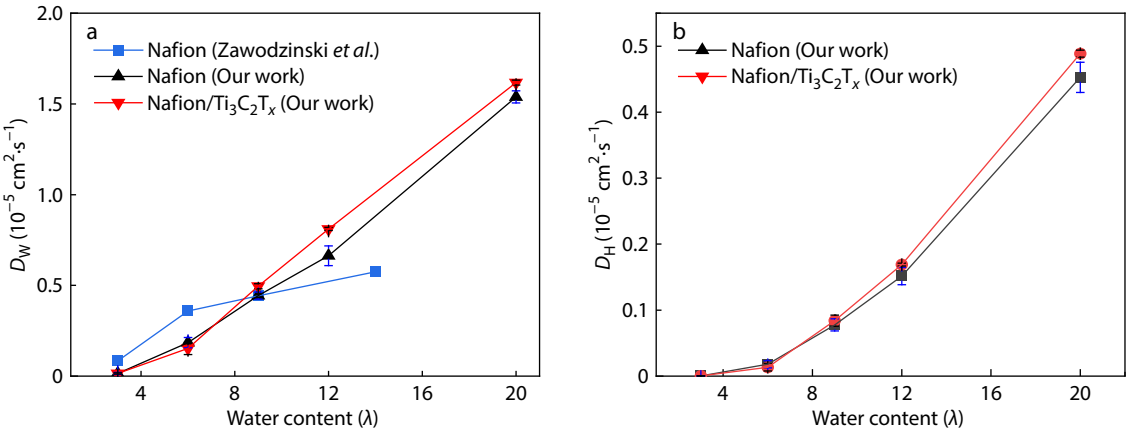

Fig. 15 The self-diffusion coefficients of water (a), and hydrated protons (b) obtained from our simulations. And the self-diffusion coefficients of water are compared with previous experimental data from Zawodzinski *et al.*[99]

Self-diffusion Coefficient of Hydrated Nafion Membranes

Proton conduction in hydrated Nafion membranes affects the conductivity and durability of fuel cells. And it is closely related to the diffusion kinetics of water molecules and hydrated protons in membranes. Therefore, we calculated the self-diffusion coefficients of water molecules (D_W) and hydrated protons (D_H) in Nafion and Nafion/$Ti_3C_2T_x$. And the calculation process is based on the simulated data in the MSD curve shown in Figs. S2 and S3 (in ESI).

As shown in Fig. 15, the variation trend of simulation data of pure Nafion membrane is basically consistent with the existing experimental data,[99] which proves the reliability of the simulation model. And the D_W and D_H in Nafion increase with increasing water content. When $Ti_3C_2T_x$ is added into Nafion, the slower diffusion of water and hydrated protons occurs at low water content (λ=3, 6). However, the diffusion of water and hydrated protons is faster at higher water content (λ=9, 12 and 20). This comes under the influence of the different microstructure and hydrogen bonds kinetics with different water content. At higher water content, the spatial distribution range of water molecules in membranes is wider. And $Ti_3C_2T_x$ in membrane are surrounded by ambient water molecules to form a hydration layer, which separates the Nafion polymer region from the $Ti_3C_2T_x$ region. Then, a relatively more continuous proton transport channel is formed between Nafion polymer and $Ti_3C_2T_x$ monomer. The continuous proton transport channel can increase the number of proton binding sites while achieving high proton conductivity and high water mobility at higher hydration levels. The current results indicate that the addition of hydrophilic material $Ti_3C_2T_x$ can improve the transport environment of water and hydrated protons, and then enhance the proton conductivity. This is in agreement with experimental study of Liu *et al.* for $Ti_3C_2T_x$ doped Nafion membrane.[40]

CONCLUSIONS

In conclusion, molecular dynamics (MD) simulation has been used to investigate the microscopic morphology and proton transport behaviors of Nafion/$Ti_3C_2T_x$ composite membrane at the molecular level. And the results indicate that there are significant differences about the diffusion kinetics of water molecules and hydronium ions in Nafion/$Ti_3C_2T_x$ at low and high hydration levels in the nanoscale region. The addition of $Ti_3C_2T_x$ into the Nafion matrix has little effect on the distribution of water molecules and hydronium ions around sulfonic acid groups. However, with the increase of water content, $Ti_3C_2T_x$ in membrane is gradually surrounded by ambient water molecules to form a hydration layer, and forming a relatively continuous proton transport channel between Nafion polymer and $Ti_3C_2T_x$ monomer. The continuous proton transport channel can increase the number of proton binding sites and thus achieving high proton conductivity and high water mobility at higher hydration level.

Hence, a relatively faster diffusion of water and hydrated protons in membrane can be achieved simultaneously. The current work can provide a theoretical guidance for designing new type of Nafion composite membranes experimentally.

Conflict of Interests

The authors declare no interest conflict.

Electronic Supplementary Information

Electronic supplementary information (ESI) is available free of charge in the online version of this article at http://doi.org/10.1007/s10118-024-3063-2.

ACKNOWLEDGMENTS

This work was financially supported by the National Key R&D Program of China (Nos. 2020YFB1505500 and 2020YFB1505503). We gratefully acknowledge HZWTECH for providing computation facilities. C. Y. thanks Shuoqi Sun for help and discussions regarding this study.

REFERENCES

1 Xu, T. C.; Wang, C. S.; Hu, Z. Y.; Zheng, J. J.; Jiang, S. H.; He, S. J.;

Hou, H. Q. High strength and stable proton exchange membrane based on perfluorosulfonic acid/polybenzimidazole. *Chinese J. Polym. Sci.* **2022**, *40*, 764–771.
2 Jiao, K.; Xuan, J.; Du, Q.; Bao, Z.; Xie, B.; Wang, B.; Zhao, Y.; Fan, L.; Wang, H.; Hou, Z.; Huo, S.; Brandon, N. P.; Yin, Y.; Guiver, M. D. Designing the next generation of proton-exchange membrane fuel cells. *Nature* **2021**, *595*, 361–369.
3 Tellez Cruz, M. M.; Escorihuela, J.; Solorza Feria, O.; Compan, V. Proton exchange membrane fuel cells (PEMFCs): advances and challenges. *Polymers* **2021**, *13*, 3046.
4 Hua, Z.; Zheng, Z.; Pahon, E.; Péra, M. C.; Gao, F. A review on lifetime prediction of proton exchange membrane fuel cells system. *J. Power Sources* **2022**, *529*, 231256.
5 Chen, X.; Xiao, L.; Qiu, X. S.; Chen, K. C. Properties of multiblock sulfonated poly(arylene ether sulfone)s synthesized by precise controllable post-sulfonation for proton exchange membranes. *Chinese J. Polym. Sci.* **2022**, *40*, 754–763.
6 Kusoglu, A.; Weber, A. Z. New insights into perfluorinated sulfonic-acid ionomers. *Chem. Rev.* **2017**, *117*, 987–1104.
7 Okonkwo, P. C.; Ben Belgacem, I.; Emori, W.; Uzoma, P. C. Nafion degradation mechanisms in proton exchange membrane fuel cell (PEMFC) system: a review. *Int. J. Hydrogen Energy* **2021**, *46*, 27956–27973.
8 Pan, M.; Pan, C.; Li, C.; Zhao, J. A review of membranes in proton exchange membrane fuel cells: transport phenomena, performance and durability. *Renew. Sust. Energy Rev.* **2021**, *141*, 110771.
9 Hickner, M. A.; Ghassemi, H.; Kim, Y. S.; Einsla, B. R.; McGrath, J. E. Alternative polymer systems for proton exchange membranes (PEMs). *Chem. Rev.* **2004**, *104*, 4587–4612.
10 Yang, C. A comparison of physical properties and fuel cell performance of Nafion and zirconium phosphate/Nafion composite membranes. *J. Membr. Sci.* **2004**, *237*, 145–161.
11 He, H.; Zhu, Y.; Li, T.; Song, S.; Zhai, L.; Li, X.; Wu, L.; Li, H. Supramolecular anchoring of polyoxometalate amphiphiles into Nafion nanophases for enhanced proton conduction. *ACS Nano* **2022**, *16*, 19240–19252.
12 Liu, Q.; Li, Z.; Wang, D.; Li, Z.; Peng, X.; Liu, C.; Zheng, P. Metal organic frameworks modified proton exchange membranes for fuel cells. *Front. Chem.* **2020**, *8*, 694.
13 Beauger, C.; Lainé, G.; Burr, A.; Taguet, A.; Otazaghine, B. Improvement of Nafion®-sepiolite composite membranes for PEMFC with sulfo-fluorinated sepiolite. *J. Membr. Sci.* **2015**, *495*, 392–403.
14 Tsai, C. H.; Wang, C. C.; Chang, C. Y.; Lin, C. H.; Chen Yang, Y. W. Enhancing performance of Nafion®-based PEMFC by 1-D channel metal-organic frameworks as PEM filler. *Int. J. Hydrogen Energy* **2014**, *39*, 15696–15705.
15 Liu, X.; Yuan, H.; Wang, C.; Zhang, S.; Zhang, L.; Liu, X.; Liu, F.; Zhu, X.; Rohani, S.; Ching, C.; Lu, J. A novel PVDF/PFSA-*g*-GO ultrafiltration membrane with enhanced permeation and antifouling performances. *Sep. Purif. Technol.* **2020**, *233*, 116038.
16 Wang, C.; Zhang, L.; Yuan, H.; Fu, Y.; Zeng, Z.; Lu, J. Preparation of a PES/PFSA-*g*-MWCNT ultrafiltration membrane with improved permeation and antifouling properties. *New J. Chem.* **2021**, *45*, 4950–4962.
17 Hao, J.; Li, X.; Yu, S.; Jiang, Y.; Luo, J.; Shao, Z.; Yi, B. Development of proton-conducting membrane based on incorporating a proton conductor 1,2,4-triazolium methanesulfonate into the Nafion membrane. *J. Energy Chem.* **2015**, *24*, 199–206.
18 Lu, Y. H.; Cao, Y.; Lu, Y. W.; Yang, T. Thermal stability and lifetime of [AMIM]Cl-PFSA composite membranes. *J. Therm. Anal. Calorim.* **2017**, *128*, 1601–1615.
19 Yin, C.; Li, J.; Zhou, Y.; Zhang, H.; Fang, P.; He, C. Enhancement in proton conductivity and thermal stability in Nafion membranes induced by incorporation of sulfonated carbon nanotubes. *ACS Appl. Mater. Interfaces* **2018**, *10*, 14026–14035.
20 Vinothkannan, M.; Kim, A. R.; Gnana Kumar, G.; Yoo, D. J. Sulfonated graphene oxide/Nafion composite membranes for high temperature and low humidity proton exchange membrane fuel cells. *RSC Adv.* **2018**, *8*, 7494–7508.
21 Wang, H.; Sun, N.; Xu, X.; Wang, S.; Kang, W.; Zhuang, X.; Yin, Y.; Cheng, B. Adenosine triphosphate@graphene oxide proton channels for proton exchange membranes constructed *via* electrostatic layer-by-layer deposition. *J. Membr. Sci.* **2021**, *620*, 118880.
22 Yao, J.; Xu, G.; Zhao, Z.; Guo, J.; Li, S.; Cai, W.; Zhang, S. An enhanced proton conductivity and reduced methanol permeability composite membrane prepared by sulfonated covalent organic nanosheets/Nafion. *Int. J. Hydrogen Energy* **2019**, *44*, 24985–24996.
23 Prapainainar, P.; Pattanapisutkun, N.; Prapainainar, C.; Kongkachuichay, P. Incorporating graphene oxide to improve the performance of Nafion-mordenite composite membranes for a direct methanol fuel cell. *Int. J. Hydrogen Energy* **2019**, *44*, 362–378.
24 Al Munsur, A. Z.; Goo, B. H.; Kim, Y.; Kwon, O. J.; Paek, S. Y.; Lee, S. Y.; Kim, H. J.; Kim, T. H. Nafion-based proton-exchange membranes built on cross-linked semi-interpenetrating polymer networks between poly(acrylic acid) and poly(vinyl alcohol). *ACS Appl. Mater. Interfaces* **2021**, *13*, 28188–28200.
25 Ryu, S.; Lee, B.; Kim, J. H.; Pak, C.; Moon, S. H. High-temperature operation of PEMFC using pore-filling PTFE/Nafion composite membrane treated with electric field. *Int. J. Energy Res.* **2021**, *45*, 19136–19146.
26 Ru, C.; Gu, Y.; Duan, Y.; Zhao, C.; Na, H. Enhancement in proton conductivity and methanol resistance of Nafion membrane induced by blending sulfonated poly(arylene ether ketones) for direct methanol fuel cells. *J. Membr. Sci.* **2019**, *573*, 439–447.
27 Ru, C.; Gu, Y.; Duan, Y.; Na, H.; Zhao, C. Nafion based semi-interpenetrating polymer network membranes from a cross-linkable SPAEK and a fluorinated epoxy resin for DMFCs. *Electrochim. Acta* **2019**, *324*, 134873.
28 Gong, K.; Zhou, K.; Qian, X.; Shi, C.; Yu, B. MXene as emerging nanofillers for high-performance polymer composites: a review. *Compos. B Eng.* **2021**, *217*, 108867.
29 Yang, Q.; Eder, S. J.; Martini, A.; Grützmacher, P. G. Effect of surface termination on the balance between friction and failure of $Ti_3C_2T_x$ MXenes. *NPJ Mater. Degrad.* **2023**, *7*, 6.
30 Tunesi, M. M.; Soomro, R. A.; Han, X.; Zhu, Q.; Wei, Y.; Xu, B. Application of MXenes in environmental remediation technologies. *Nano Converg.* **2021**, *8*, 5.
31 Soleymaniha, M.; Shahbazi, M. A.; Rafieerad, A. R.; Maleki, A.; Amiri, A. Promoting role of MXene nanosheets in biomedical sciences: therapeutic and biosensing innovations. *Adv. Healthc. Mater.* **2019**, *8*, 1801137.
32 Huang, K.; Li, Z.; Lin, J.; Han, G.; Huang, P. Two-dimensional transition metal carbides and nitrides (MXenes) for biomedical applications. *Chem. Soc. Rev.* **2018**, *47*, 5109–5124.
33 Pandey, R. P.; Rasool, K.; Madhavan, V. E.; Aïssa, B.; Gogotsi, Y.; Mahmoud, K. A. Ultrahigh-flux and fouling-resistant membranes based on layered silver/MXene ($Ti_3C_2T_x$) nanosheets. *J. Mater. Chem. A* **2018**, *6*, 3522–3533.
34 Zhou, H.; Han, S. J.; Lee, H. D.; Zhang, D.; Anayee, M.; Jo, S. H.; Gogotsi, Y.; Lee, T. W. Overcoming the limitations of MXene electrodes for solution-processed optoelectronic devices. *Adv. Mater.* **2022**, *34*, 2206377.
35 Wang, J.; Zhai, P.; Zhao, T.; Li, M.; Yang, Z.; Zhang, H.; Huang, J. Laminar MXene-Nafion-modified separator with highly inhibited shuttle effect for long-life lithium-sulfur batteries. *Electrochim.*

Acta **2019**, *320*, 134558.
36 Jang, J.; Kang, Y.; Kim, K.; Kim, S.; Son, M.; Chee, S. S.; Kim, I. S. Concrete-structured Nafion@MXene/Cellulose acetate cation exchange membrane for reverse electrodialysis. *J. Membr. Sci.* **2022**, *646*, 120239.
37 Tang, X.; Zhou, Z.; Jiang, Y.; Wang, Q.; Sun, Q.; Zu, L.; Gao, X.; Lian, H.; Cao, M.; Cui, X. MXene enhanced the electromechanical performance of a Nafion-based actuator. *Materials* **2022**, *15*, 2833.
38 Lee, S. J.; Lee, D. H.; Lee, W. Y. An electrochemical sensor for capsaicin based on two-dimensional titanium carbide (MXene)-doped titania-Nafion composite film. *Microchem. J.* **2023**, *185*, 108216.
39 Guan, P.; Lei, J.; Zou, Y.; Zhang, Y. Improved thermo-mechanical properties and reduced hydrogen permeation of short side-chain perfluorosulfonic acid membranes doped with $Ti_3C_2T_x$. *Materials* **2021**, *14*, 7875.
40 Liu, Y.; Zhang, J.; Zhang, X.; Li, Y.; Wang, J. $Ti_3C_2T_x$ filler effect on the proton conduction property of polymer electrolyte membrane. *ACS Appl. Mater. Interfaces* **2016**, *8*, 20352–20363.
41 Savage, J.; Tse, Y. L. S.; Voth, G. A. Proton transport mechanism of perfluorosulfonic acid membranes. *J. Phys. Chem. C* **2014**, *118*, 17436–17445.
42 Li, J.; Jin, S. H.; Lan, G. C.; Xu, Z. S.; Wang, L. T.; Wang, N.; Li, L. J. Research on the glass transition temperature and mechanical properties of poly(vinyl chloride)/dioctyl phthalate (PVC/DOP) blends by molecular dynamics simulations. *Chinese J. Polym. Sci.* **2019**, *37*, 834–840.
43 Wang, D. D.; Yu, K. F.; Xu, X. L.; Xu, W. S. Molecular dynamics study of star polymer melts under start-up shear. *Chinese J. Polym. Sci.* **2022**, *40*, 807–816.
44 Kritikos, G.; Pant, R.; Sengupta, S.; Karatasos, K.; Venkatnathan, A.; Lyulin, A. V. Nanostructure and dynamics of humidified Nafion/graphene-oxide composites *via* molecular dynamics simulations. *J. Phys. Chem. C* **2018**, *122*, 22864–22875.
45 Mabuchi, T.; Tokumasu, T. Relationship between proton transport and morphology of perfluorosulfonic acid membranes: a reactive molecular dynamics approach. *J. Phys. Chem. B* **2018**, *122*, 5922–5932.
46 Akbari, S.; Mosavian, M. T. H.; Moosavi, F.; Ahmadpour, A. Does the addition of a heteropoly acid change the water percolation threshold of PFSA membranes. *Phys. Chem. Chem. Phys.* **2019**, *21*, 25080–25089.
47 Savage, J.; Voth, G. A. Proton solvation and transport in realistic proton exchange membrane morphologies. *J. Phys. Chem. C* **2016**, *120*, 3176–3186.
48 Kuo, A. T.; Urata, S.; Nakabayashi, K.; Watabe, H.; Honmura, S. Coarse-grained molecular dynamics simulation of perfluorosulfonic acid polymer in water-ethanol mixtures. *Macromolecules* **2021**, *54*, 609–620.
49 Tarokh, A.; Karan, K.; Ponnurangam, S. Atomistic MD study of Nafion dispersions: role of solvent and counterion in the aggregate structure, ionic clustering, and acid dissociation. *Macromolecules* **2019**, *53*, 288–301.
50 Kuo, A. T.; Takeuchi, K.; Tanaka, A.; Urata, S.; Okazaki, S.; Shinoda, W. Exploring the effect of pendent side chain length on the structural and mechanical properties of hydrated perfluorosulfonic acid polymer membranes by molecular dynamics simulation. *Polymer* **2018**, *146*, 53–62.
51 Kuo, A. T.; Shinoda, W.; Okazaki, S. Molecular dynamics study of the morphology of hydrated perfluorosulfonic acid polymer membranes. *J. Phys. Chem. C* **2016**, *120*, 25832–25842.
52 Takeuchi, K.; Kuo, A. T.; Hirai, T.; Miyajima, T.; Urata, S.; Terazono, S.; Okazaki, S.; Shinoda, W. Hydrogen permeation in hydrated perfluorosulfonic acid polymer membranes: effect of polymer crystallinity and equivalent weight. *J. Phys. Chem. C* **2019**, *123*, 20628–20638.
53 Cui, R.; Li, S.; Yu, C.; Wang, Y.; Zhou, Y. Understanding the mechanism of nitrogen transport in the perfluorinated sulfonic-acid hydrated membranes *via* molecular dynamics simulations. *J. Membr. Sci.* **2022**, *648*, 120328.
54 Fan, L.; Xi, F.; Wang, X.; Xuan, J.; Jiao, K. Effects of side chain length on the structure, oxygen transport and thermal conductivity for perfluorosulfonic acid membrane: molecular dynamics simulation. *J. Electrochem. Soc.* **2019**, *166*, F511–F518.
55 Ban, S.; Huang, C.; Yuan, X. Z.; Wang, H. Molecular simulation of gas transport in hydrated Nafion membranes: influence of aqueous nanostructure. *J. Phys. Chem. C* **2012**, *116*, 17424–17430.
56 Ban, S.; Huang, C.; Yuan, X. Z.; Wang, H. Molecular simulation of gas adsorption, diffusion, and permeation in hydrated Nafion membranes. *J. Phys. Chem. B* **2011**, *115*, 11352–11358.
57 Cui, R.; Li, S.; Yu, C.; Zhou, Y. The evolution of hydrogen bond network in Nafion *via* molecular dynamics simulation. *Macromolecules* **2023**, *56*, 1688–1703.
58 Sun, S.; Ling, L.; Xiong, Y.; Zhang, Y.; Li, Z. Trifluoromethanesulfonimide-based hygroscopic semi-interpenetrating polymer network for enhanced proton conductivity of Nafion-based proton exchange membranes at low humidity. *J. Membr. Sci.* **2020**, *612*, 118339.
59 Atrazhev, V. V.; Astakhova, T. Y.; Sultanov, V. I.; Perry, M. L.; Burlatsky, S. F. Molecular dynamic study of water-cluster structure in PFSA and PFIA ionomers. *J. Electrochem. Soc.* **2017**, *164*, F1265–F1271.
60 Li, Z. Z.; Chen, L.; Tao, W. Q. Molecular dynamics simulation of water permeation through the Nafion membrane. *Numer. Heat Tr. A-Appl.* **2016**, *70*, 1232–1241.
61 Daly, K. B.; Benziger, J. B.; Debenedetti, P. G.; Panagiotopoulos, A. Z. Molecular dynamics simulations of water sorption in a perfluorosulfonic acid membrane. *J. Phys. Chem. B* **2013**, *117*, 12649–12660.
62 Gonçalves, W.; Mabuchi, T.; Tokumasu, T. Nucleation and growth of cavities in hydrated Nafion membranes under tensile strain: a molecular dynamics study. *J. Phys. Chem. C* **2019**, *123*, 28958–28968.
63 Kuo, A. T.; Miyazaki, Y.; Jang, C.; Miyajima, T.; Urata, S.; Nielsen, S. O.; Okazaki, S.; Shinoda, W. Large-scale molecular dynamics simulation of perfluorosulfonic acid membranes: remapping coarse-grained to all-atomistic simulations. *Polymer* **2019**, *181*, 121766.
64 Kuo, A. T.; Tanaka, A.; Irisawa, J.; Shinoda, W.; Okazaki, S. Molecular dynamics study on the mechanical deformation of hydrated perfluorosulfonic acid polymer membranes. *J. Phys. Chem. C* **2017**, *121*, 21374–21382.
65 Xie, J.; Ban, S.; Liu, B.; Zhou, H. A molecular simulation study of chemical degradation and mechanical deformation of hydrated Nafion membranes. *Appl. Surf. Sci.* **2016**, *362*, 441–447.
66 Maiti, T. K.; Singh, J.; Maiti, S. K.; Majhi, J.; Ahuja, A.; Singh, M.; Bandyopadhyay, A.; Manik, G.; Chattopadhyay, S. Molecular dynamics simulations and experimental studies of the perfluorosulfonic acid-based composite membranes containing sulfonated graphene oxide for fuel cell applications. *Eur. Polym. J.* **2022**, *174*, 111345.
67 Haghighi Asl, M.; Moosavi, F.; Akbari, S. Mixed membrane matrices (MMMs) based on Nafion® pristine/defected-UiO-66(Zr) MOFs: assessment of the effects of dopants on cluster morphology. *Mol. Syst. Des. Eng.* **2022**, *7*, 969–985.
68 Liu, Y.; Sambasivarao, S. V.; Horan, J. L.; Yang, Y.; Maupin, C. M.; Herring, A. M. A combined theoretical and experimental investigation of the transport properties of water in a

perfluorosulfonic acid proton exchange membrane doped with the heteropoly acids, $H_3PW_{12}O_{40}$ or $H_4SiW_{12}O_{40}$. *J. Phys. Chem. C* **2013**, *118*, 854–863.
69 Sambasivarao, S. V.; Liu, Y.; Horan, J. L.; Seifert, S.; Herring, A. M.; Maupin, C. M. Enhancing proton transport and membrane lifetimes in perfluorosulfonic acid proton exchange membranes: a combined computational and experimental evaluation of the structure and morphology changes due to $H_3PW_{12}O_{40}$ doping. *J. Phys. Chem. C* **2014**, *118*, 20193–20202.
70 Akbari, S.; Hamed Mosavian, M. T.; Moosavi, F.; Ahmadpour, A. Elucidating the morphological aspects and proton dynamics in a hybrid perfluorosulfonic acid membrane for medium-temperature fuel cell applications. *Phys. Chem. Chem. Phys.* **2018**, *20*, 29778–29789.
71 Akbari, S.; Hamed Mosavian, M. T.; Moosavi, F.; Ahmadpour, A. Atomistic simulation of proton transfer ability of isopoly acid (IPA)/heteropoly acid (HPA) doped Nafion® 117 for high-temperature fuel cell applications. *Compos. B Eng.* **2019**, *161*, 402–410.
72 Lee, O. S.; Madjet, M. E.; Mahmoud, K. A. Antibacterial mechanism of multifunctional MXene nanosheets: domain formation and phase transition in lipid bilayer. *Nano Lett.* **2021**, *21*, 8510–8517.
73 Hope, M. A.; Forse, A. C.; Griffith, K. J.; Lukatskaya, M. R.; Ghidiu, M.; Gogotsi, Y.; Grey, C. P. NMR reveals the surface functionalisation of Ti_3C_2 MXene. *Phys. Chem. Chem. Phys.* **2016**, *18*, 5099–5102.
74 Martinez, L.; Andrade, R.; Birgin, E. G.; Martinez, J. M. PACKMOL: a package for building initial configurations for molecular dynamics simulations. *J. Comput. Chem.* **2009**, *30*, 2157–2164.
75 Wang, C.; Clark, J. K.; Kumar, M.; Paddison, S. J. An ab initio study of the primary hydration and proton transfer of CF_3SO_3H and $CF_3O(CF_2)_2SO_3H$: effects of the hybrid functional and inclusion of diffuse functions. *Solid State Ion*. **2011**, *199–200*, 6–13.
76 Mabuchi, T.; Tokumasu, T. Effect of bound state of water on hydronium ion mobility in hydrated Nafion using molecular dynamics simulations. *J. Chem. Phys.* **2014**, *141*, 104904.
77 Levitt, M.; Hirshberg, M.; Sharon, R.; Laidig, K. E.; Daggett, V. Calibration and testing of a water model for simulation of the molecular dynamics of proteins and nucleic acids in solution. *J. Phys. Chem. B* **1997**, *101*, 5051–5061.
78 Jang, S. S.; Molinero, V.; Çağın, T.; Goddard, W. A. Nanophase-segregation and transport in Nafion 117 from molecular dynamics simulations: effect of monomeric sequence. *J. Phys. Chem. B* **2004**, *108*, 3149–3157.
79 Rappe, A. K.; Casewit, C. J.; Colwell, K. S.; Goddard, W. A.; Skiff, W. M. UFF, a full periodic table force field for molecular mechanics and molecular dynamics simulations. *J. Am. Chem. Soc.* **2002**, *114*, 10024–10035.
80 Hu, T.; Wang, J.; Zhang, H.; Li, Z.; Hu, M.; Wang, X. Vibrational properties of Ti_3C_2 and $Ti_3C_2T_2$ (T = O, F, OH) monosheets by first-principles calculations: a comparative study. *Phys. Chem. Chem. Phys.* **2015**, *17*, 9997–10003.
81 Xu, K.; Lin, Z.; Merlet, C.; Taberna, P. L.; Miao, L.; Jiang, J.; Simon, P. Tracking ionic rearrangements and interpreting dynamic volumetric changes in two-dimensional metal carbide supercapacitors: a molecular dynamics simulation study. *ChemSusChem* **2018**, *11*, 1892–1899.
82 Abraham, M. J.; Murtola, T.; Schulz, R.; Páll, S.; Smith, J. C.; Hess, B.; Lindahl, E. GROMACS: high performance molecular simulations through multi-level parallelism from laptops to supercomputers. *Softwarex* **2015,** *1–2*, 19–25.
83 Martyna, G. J.; Klein, M. L.; Tuckerman, M. Nosé-Hoover chains: the canonical ensemble *via* continuous dynamics. *J. Chem. Phys.* **1992**, *97*, 2635–2643.
84 Parrinello, M.; Rahman, A. Polymorphic transitions in single crystals: a new molecular dynamics method. *J. Appl. Phys.* **1981**, *52*, 7182–7190.
85 Essmann, U.; Perera, L.; Berkowitz, M. L.; Darden, T.; Lee, H.; Pedersen, L. G. A smooth particle mesh Ewald method. *J. Chem. Phys.* **1995**, *103*, 8577–8593.
86 Liu, W.; Hong, G.; Dai, D.; Li, L.; Dolg, M. The Beijing four-component density functional program package (BDF) and its application to EuO, EuS, YbO and YbS. *Theor. Chem. Acc.* **1997**, *96*, 75–83.
87 Zhang, Y.; Suo, B.; Wang, Z.; Zhang, N.; Li, Z.; Lei, Y.; Zou, W.; Gao, J.; Peng, D.; Pu, Z.; Xiao, Y.; Sun, Q.; Wang, F.; Ma, Y.; Wang, X.; Guo, Y.; Liu, W. BDF: a relativistic electronic structure program package. *J. Chem. Phys.* **2020**, *152*, 064113.
88 Liu, W. J.; Wang, F.; Li, L. M. The Beijing Density Functional (BDF) program package: methodologies and applications. *J. Theor. Comput. Chem.* **2003**, *2*, 257–272.
89 Liu, W. J.; Wang, F.; Li, L. *Relativistic Density Functional Theory: The BDF Program Package*. World Scientific, Singapore, **2004**, p. 257–282.
90 Wang, Z.; Li, Z.; Zhang, Y.; Liu, W. Analytic energy gradients of spin-adapted open-shell time-dependent density functional theory. *J. Chem. Phys.* **2020**, *153*, 164109.
91 Hongzhiwei Technology, Device Studio, Version 2023A, China, 2023. Available online: https://cloud.hzwtech.com/web/product-service?id=6 (accessed on Aug., 23rd).
92 Morris, D. R.; Sun, X. Water-sorption and transport properties of Nafion 117. *J. Appl. Polym. Sci.* **1993**, *50*, 1445–1452.
93 Weber, A. Z.; Newman, J. Transport in polymer-electrolyte membranes: II. Mathematical model. *J. Electrochem. Soc.* **2004**, *151*, A311–A325.
94 Ohkubo, T.; Kidena, K.; Takimoto, N.; Ohira, A. Molecular dynamics simulations of Nafion and sulfonated polyether sulfone membranes. I. Effect of hydration on aqueous phase structure. *J. Mol. Model.* **2011**, *17*, 739–755.
95 Liu, J.; Suraweera, N.; Keffer, D. J.; Cui, S.; Paddison, S. J. On the relationship between polymer electrolyte structure and hydrated morphology of perfluorosulfonic acid membranes. *J. Phys. Chem. C* **2010**, *114*, 11279–11292.
96 Dixit, S.; Crain, J.; Poon, W. C.; Finney, J. L.; Soper, A. K. Molecular segregation observed in a concentrated alcohol-water solution. *Nature* **2002**, *416*, 829–832.
97 Zhou, A.; Liu, Y.; Li, S.; Wang, X.; Ying, G.; Xia, Q.; Zhang, P. From structural ceramics to 2D materials with multi-applications: a review on the development from MAX phases to MXenes. *J. Adv. Ceram.* **2021**, *10*, 1194–1242.
98 Devanathan, R.; Venkatnathan, A.; Rousseau, R.; Dupuis, M.; Frigato, T.; Gu, W.; Helms, V. Atomistic simulation of water percolation and proton hopping in Nafion fuel cell membrane. *J. Phys. Chem. B* **2010**, *114*, 13681–13690.
99 Zawodzinski, T. A.; Neeman, M.; Sillerud, L. O.; Gottesfeld, S. Determination of water diffusion coefficients in perfluorosulfonate ionomeric membranes. *J. Phys. Chem.* **1991**, *95*, 6040–6044.

https://doi.org/10.1007/s10118-024-3063-2